INTERFACE SCIENCE 11, 131–148, 2003

Atomistic Modeling of Point Defects and Diffusion in Copper Grain Boundaries

A. SUZUKI AND Y. MISHIN
School of Computational Sciences, MSN 5C3, George Mason University, Fairfax, VA 22030-4444, USA

Abstract. The atomic structure of several symmetrical tilt grain boundaries (GBs) in Cu and their interaction with vacancies and interstitials as well as self-diffusion are studied by molecular statics, molecular dynamics, kinetic Monte Carlo (KMC), and other atomistic simulation methods. Point defect formation energy in the GBs is on average lower than in the lattice but variations from site to site within the GB core are very significant. The formation energies of vacancies and interstitials are close to one another, which makes the defects equally important for GB diffusion. Vacancies show interesting effects such as delocalization and instability at certain GB sites. They move in GBs by simple vacancy-atom exchanges or by "long jumps" involving several atoms. Interstitial atoms can occupy relatively open positions between atoms, form split dumbbell configurations, or form highly delocalized displacement zones. They diffuse by direct jumps or by the indirect mechanism involving a collective displacement of several atoms. Diffusion coefficients in the GBs have been calculated by KMC simulations using defect jump rates determined within the transition state theory. GB diffusion can be dominated by vacancies or interstitials, depending on the GB structure. The diffusion anisotropy also depends on the GB structure, with diffusion along the tilt axis being either faster or slower than diffusion normal to the tilt axis. In agreement with Borisov's correlation, the activation energy of GB diffusion tends to decrease with the GB energy.

Keywords: grain boundary, point defects, diffusion, computer modeling

1. Introduction

Grain boundary (GB) diffusion controls the kinetics of many microstructural changes, phase transformations, solid-state reactions, creep, and other processes in solid materials at elevated temperatures [1]. For many technological applications it is important to be able to predict diffusion coefficients in GBs by calculation. A prerequisite of such calculations is a knowledge of atomic mechanisms by which point defects move in GBs. Because existing experimental methods do not provide direct information on GB diffusion on the atomic level, the current knowledge of diffusion mechanisms comes primarily from atomistic computer modeling [2, 3].

It has been assumed since many years that atoms move in GBs predominantly by simple exchanges with vacancies, i.e., by the same mechanism as in the lattice [1, 4]. The vacancy mechanism appears to be consistent with experimental activation energies of GB diffusion and was confirmed by early atomistic simulations [5]. More recent simulations of symmetrical tilt GBs in Ag [6, 7] and Cu [8] as well as twist GBs in Cu [9, 10] revealed also an important role of self-interstitials in GB diffusion. Furthermore, recent diffusion simulations in $\Sigma = 5$ GBs in Cu [8] identified a number of collective mechanisms involving vacancies and interstitials, and even the ring mechanism which can operate without any pre-existing point defects. Vacancies in $\Sigma = 5$ GBs have been found to demonstrate interesting structural effects such as delocalization and instability at certain cites in the GB core [8].

In this paper we continue the investigation of diffusion in Cu GBs initiated in Ref. [8]. The question which we intend to address here is whether the results of Ref. [8] are specific to $\Sigma = 5$ GBs or are general and hold for other GBs as well. Another question is whether the results of Ref. [8] depend on the

embedded-atom potential used to describe atomic interactions in Cu. To answer these questions we re-examine diffusion in $\Sigma = 5$ symmetrical tilt GBs in Cu with a different embedded-atom potential and study diffusion in four other GBs with different tilt axes and GB planes. Our methodology is similar to that of Ref. [8] with slight variations. The dominant diffusion mechanisms in GBs are identified by molecular dynamics (MD), while GB diffusion coefficients are calculated by kinetic Monte Carlo (KMC) simulations. The catalog of rate constants required for KMC simulations is generated using the transition state theory of rate processes. By comparing diffusion coefficients calculated for different mechanisms, the dominant diffusion mechanism in each GB and in each diffusion direction is identified and correlations between diffusion characteristics, on one hand, and the GB structure and energy, on the other hand, are examined.

2. Grain Boundary Structure

2.1. *Interatomic Potential and Simulation Conditions*

Atomic interactions in Cu were described by an embedded-atom potential constructed in Ref. [11]. The potential accurately reproduces experimental values of the equilibrium lattice constant, cohesive energy, elastic constants, phonon frequencies, thermal expansion, vacancy formation energy, stacking fault energy, and other properties of Cu. The potential is also fit to first-principles energy-volume relations of fcc Cu and a number of alternative computer-generated structures of Cu. The incorporation of first-principles data is known to improve the transferability of potentials to various atomic configurations encountered in atomistic simulations [12].

The geometry of our simulation block is illustrated in Fig. 1. The block contains two grains joined along the GB plane which is parallel to the x and z axes. Each grain contains free (dynamic) atoms, which are able to move under interatomic forces, as well as fixed atoms which are fixed in their perfect lattice positions relative to one another. Periodic boundary conditions are applied in directions parallel to the GB plane. The slabs of fixed atoms serve to represent lattice regions far away from the GB. The slabs are able to move in a rigid-body matter in the direction normal to the GB plane in order to accommodate the local expansion of the GB core due to its presumably more open structure than the

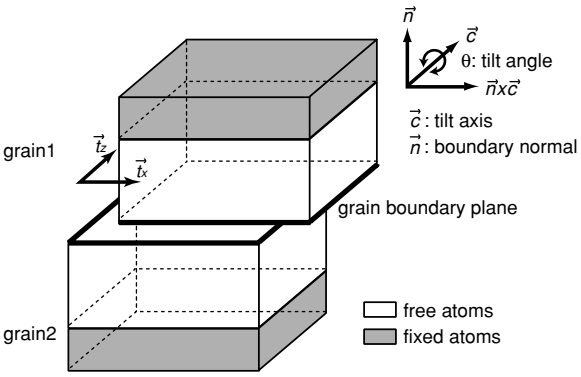

Figure 1. Schematic geometry and boundary conditions in grain boundary simulations. $\mathbf{t}_x$ and $\mathbf{t}_z$ are translation vectors parallel to the grain boundary plane.

fcc bulk. They are also allowed to move parallel to the GB plane to explore microscopic degrees of freedom of the GB. The block typically contains over a thousand free atoms.

The GB is initially created by aligning the desired crystallographic plane parallel to the intended GB plane and the tilt axis direction parallel to the z-direction. A 180° rotation of one grain relative to the other about the normal $\mathbf{n}$ to the GB plane produces a symmetrical tilt GB with a certain reciprocal density of coincidence sites Σ. Six high-angle symmetrical tilt GBs have been created and studied in this work: $\Sigma = 5(210)[001]\ \theta = 53.13°$, $\Sigma = 5(310)\,[001]\,\theta = 36.87°$, $\Sigma = 9(1\bar{2}2)[011]\ \theta = 38.94°$, $\Sigma = 11(3\bar{1}1)[011]\ \theta = 50.48°$, $\Sigma = 7(2\bar{3}1)[111]\ \theta = 38.21°$, and $\Sigma = 13(3\bar{4}1)[111]\ \theta = 27.80°$, where θ is tilt angle.

2.2. *γ Surfaces of Grain Boundaries*

The energy of each GB was minimized with respect to local atomic displacements of dynamic atoms and rigid-body translations of the grains. The energy minimization was performed by the γ surface method [13]. This method was originally developed in the context of dislocations and planar faults and recently applied to GBs [14]. In the γ surface method, the partially relaxed GB energy γ is calculated as functions of the translation vector $\mathbf{t}$ of one grain relative to the other parallel to the GB plane (see Fig. 1). The partial relaxation includes local atomic displacements and rigid translations of the grains normal to the GB plane but not parallel to it. Local minima on the γ surface $\gamma(t_x, t_z)$ correspond to relative translations of the grains producing stable

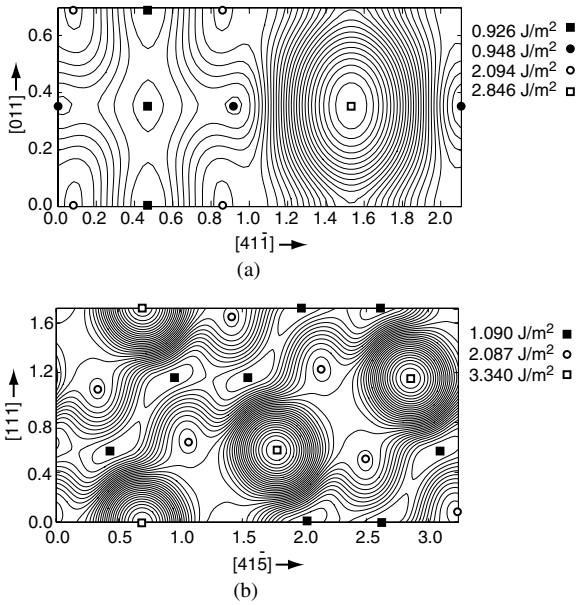

Figure 2. γ surfaces of symmetrical tilt grain boundaries in Cu. (a) $\Sigma = 9(1\bar{2}2)[011]$ GB; (b) $\Sigma = 7(2\bar{3}1)[111]$ GB. Grain translations are measured in units of the lattice parameter a. Local minima and maxima of energy are marked by filled and open symbols, respectively. The respective energies are given in the key.

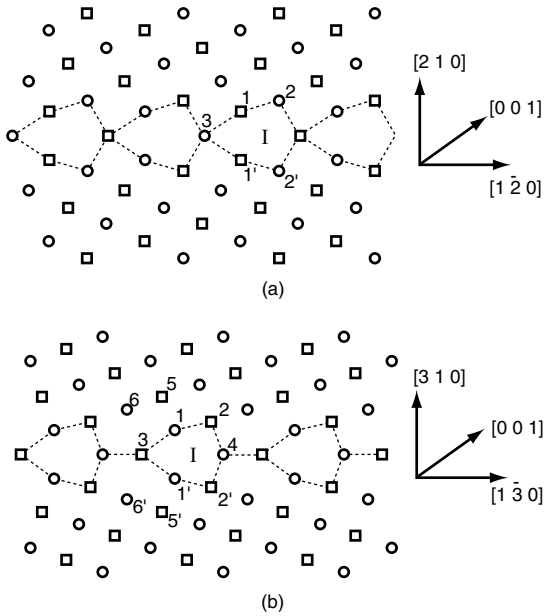

Figure 3. Relaxed atomic structure of $\Sigma = 5$ [001] symmetrical tilt grain boundaries in Cu. (a) $\theta = 53.13^\circ$ (210) GB; (b) $\theta = 36.87^\circ$ (310) GB. Circles and squares mark atomic positions in alternating (002) planes perpendicular to the tilt axis [001]. Selected atomic sites are labeled for further reference. The prime marks symmetrically equivalent sites within the same structural unit. Symbol I marks an interstitial site. Dashed lines delineate structural units.

or metastable GB structures. Such structures are examined separately by full relaxation which includes arbitrary displacements of dynamic atoms in all directions with simultaneous rigid-body displacements of the grains perpendicular to the GB plane. The deepest energy minimum corresponds to the ground state structure of the GB.

Contour plots of typical γ surfaces of GBs are illustrated in Fig. 2, where the translations t_x and t_z are measured in units of the lattice parameter a. The contours are plotted in every 0.06 to 0.08 J/m^2 depending on the complexity of the surfaces. For [111] GBs, the full relaxation results in a small shift of the energy minimum away from its position on the γ surface. For the $\Sigma = 7$ GB, this shift has a component $0.083a$ parallel to the tilt axis, with the result that (111) planes become discontinuous across the GB. In contrast, for the $\Sigma = 13$ GB the shift is normal to the tilt axis and (111) planes remain continuous.

2.3. *Atomic Structure of Grain Boundaries*

The relaxed ground state structures of the six GBs studied in this work are shown in Figs. 3, 4 and 5. The structure of $\Sigma = 5$ GBs (Fig. 3) is well known from experimental observations and previous simulations [4, 8, 15–17]. Both $\Sigma = 5$ GBs consist of topologically identical structural units which represent a capped trigonal prism in three-dimensional space. The boundaries only differ in the way the structural units are connected to each other.

The $\Sigma = 9(1\bar{2}2)[011]$ and $\Sigma = 11(3\bar{1}1)[011]$ GBs (Fig. 4) are composed of the same, although slightly distorted, capped trigonal prisms. The $\Sigma = 11$ GB is often represented by diamond-shape units, but Fig. 4(b) demonstrates that such units are nothing but fragments of capped trigonal prisms. The structures of these GBs are also in agreement with previous computer simulations [18] and experimental observations [19].

The structural units of the $\Sigma = 7(2\bar{3}1)[111]$ and $\Sigma = 13(3\bar{4}1)[111]$ GBs (Fig. 5) are capped trigonal archimedean prisms which look like hexagons in the projection normal to the tilt axis. These units are bridged in the $\Sigma = 7$ GB and interlocked in the $\Sigma = 13$ GB. The side projection of the $\Sigma = 7$ GB shown in Fig. 5(b) illustrates the discontinuity of (111) planes mentioned above. Note that the same kind of discontinuity in the $\Sigma = 7$ GB was observed by atomistic

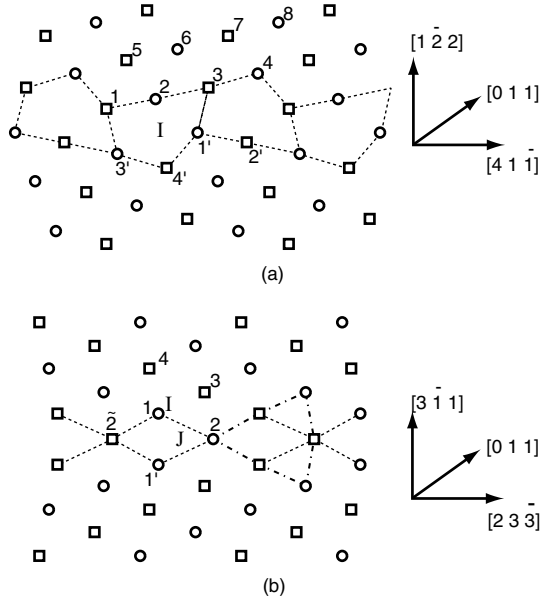

Figure 4. Relaxed atomic structure of [011] symmetrical tilt grain boundaries in Cu. (a) $\Sigma = 9(1\bar{2}2)\ \theta = 38.94^\circ$ GB; (b) $\Sigma = 11(3\bar{1}1)$ $\theta = 50.48^\circ$ GB. Circles and squares mark atomic positions in alternating (022) planes perpendicular to the tilt axis [011]. Selected atomic sites are labeled for further reference. The prime marks symmetrically equivalent sites within the same structural unit. Symbols I and J mark interstitial sites. Dashed lines delineate structural units.

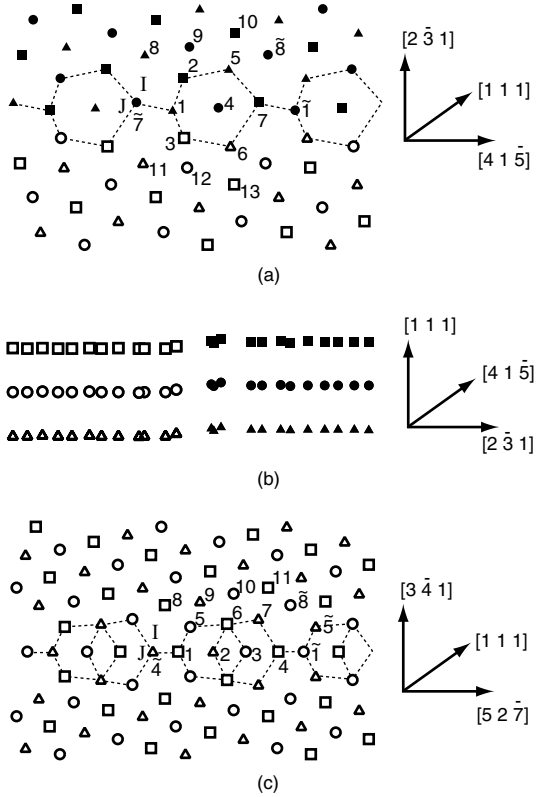

Figure 5. Relaxed atomic structure of [111] symmetrical tilt grain boundaries in Cu. Circles, squares, and triangles mark atomic positions in (333) planes perpendicular to the tilt axis [111]. (a) $\Sigma = 7(2\bar{3}1)\ \theta = 38.21^\circ$ GB, projection perpendicular to the tilt axis. (b) Same GB, projection parallel to the tilt axis. Filled symbols mark the upper grain and open symbols the lower grain. The relative shift of the grains is about 0.03 nm in the direction parallel to the tilt axis. (c) $\Sigma = 13(3\bar{4}1)\ \theta = 27.80^\circ$ GB. Selected atomic sites are labeled for further reference. Symbols I and J mark interstitial sites. Dashed lines delineate structural units.

simulations in Pd [17]. A similar structure of the $\Sigma = 7$ GB was observed by high-resolution transmission electron microscopy in Al [20].

The energies of all six GBs are summarized in Table 1. We see that the $\Sigma = 11(3\bar{1}1)[011]$ GB has the lowest energy, which fact is consistent with its highly symmetrical structure and fcc-like local configurations in the GB core.

3. Point Defects in Grain Boundaries

3.1. Point Defect Calculations

Our diffusion calculations rest on the assumption that atomic migration in GBs is mediated by the migration of individual point defects: vacancies and interstitials. This model may not apply at high temperatures at which GBs become highly disordered and the notion of point defects may lose sense [17]. Our calculations are thus relevant to diffusion at relatively low and medium temperatures at which GBs have a well-defined ordered structure and support point defects.

The first step of the work was to study the energy, entropy and structure of point defects in GBs. Bulk properties of point defects in Cu calculated with the same EAM potential are summarized in Table 2. The bulk interstitial is considered in its ground state configuration, which is a [001]-split dumbbell. The dumbbell

Table 1. Energies of Cu grain boundaries studied in this work.

GB	Tilt angle θ (°)	GB energy (J/m^2)
$\Sigma = 5(210)[001]$	53.13	0.952
$\Sigma = 5(310)[001]$	36.87	0.905
$\Sigma = 9(1\bar{2}2)[011]$	38.94	0.834
$\Sigma = 11(3\bar{1}1)[011]$	50.48	0.301
$\Sigma = 7(2\bar{3}1)[111]$	38.21	0.867
$\Sigma = 13(3\bar{4}1)[111]$	27.80	0.842

Table 2. Characteristics of point defect formation and migration in bulk Cu calculated with the present EAM potential [11] using a 864-atom simulation block with periodic boundaries. Experimental data are given in parentheses. E_f—formation energy, S_f—formation entropty, ν_0—attempt frequency.

Defect	E_f (eV)	S_f/k_B	E_m (eV)	ν_0 (THz)
Vacancy	1.272	1.399	0.689	7.6
	(1.27[a];1.28[b])	(2.35[c])	(0.71[b])	
Interstitial	3.066	7.429	0.098	2.0
	(2.8–4.2[c])		(0.12[d])	

[a]Reference [21].
[b]Reference [22].
[c]Reference [23].
[d]Reference [24].

moves by a collective jump of three atoms in which the center of mass of the dumbbell translates by vector (1/2)[110] with a simultaneous 90° rotation of the dumbbell in the (001) plane to the [010] orientation. The numbers reported in Table 2 were calculated by including both atomic and volume relaxation of the simulation block.

The defect formation energy E_f^α at a particular site α in the GB core is determined from the equation

$$E_f^\alpha = E_{GB}^\alpha - E_{GB} \pm \frac{E_{bulk}}{N}, \tag{1}$$

where the positive sign refers to a vacancy and the negative sign to an interstitial. Here N is the number of dynamic atoms in the simulation block, E_{GB}^α is the energy of a $(N \pm 1)$-atom simulation block with a point defect at site α, E_{GB} is the energy of the initial N-atom block with a GB but without the defect, and E_{bulk} is the energy of an N-atom perfect lattice block. Thus, the vacancy formation energy in a GB has the meaning of the energy cost of removing an atom from a GB site α and placing it at a perfect lattice site far away from the GB. The interstitial formation energy has a similar meaning except that the atom is moved from the perfect lattice to the GB. The energies E_{GB}^α and E_{GB} are determined after a static relaxation of the simulation block including both atomic displacements and rigid-body translations of the grains (Fig. 1).

The point defect formation entropy was calculated in the classical harmonic approximation in which the vibrational entropy S of a system of N dynamic atoms at a temperature T is given by

$$S = k_B \sum_{i=1}^{3N} \ln\left(\frac{k_B T}{h\nu_i}\right) + 3Nk_B. \tag{2}$$

Here ν_i are the frequencies of normal atomic vibrations determined by diagonalizing the dynamical matrix of the system, k_B is the Boltzmann constant, and h is the Plank constant. The defect formation entropy is determined from the difference in the entropy of a simulation block with and without a point defect under constant N conditions. As with the defect energy, the formula of the defect formation entropy S_f^α at a GB site α is

$$S_f^\alpha = S_{GB}^\alpha - S_{GB} \pm \frac{S_{bulk}}{N}. \tag{3}$$

Here S_{GB}^α is the entropy of a $(N \pm 1)$-atom simulation block with a point defect at site α, S_{GB} is the entropy of the initial N-atom block with a GB but without the defects, and S_{bulk} is the entropy of an N-atom perfect lattice block. Note that the $k_B T$ factor cancels out in Eq. (3), so that S_f^α does not depend on temperature.[1]

The obtained energies and entropies of point defects at selected GB sites are summarized in Table 3. In Fig. 6, the vacancy formation energy is plotted as a function of the distance from the GB for all six GBs studied here. Two observations can be made from these plots. First, all deviations of the vacancy formation energy from the bulk value are highly localized within a relatively narrow (±0.5 nm) core region. Beyond that region the energy practically coincides with its undisturbed bulk value. Second, the vacancy formation energy in the GB core is highly non-uniform, the fact which is also evident from Table 3. It can be as low as 20% of the bulk value at some sites and higher than the bulk value at other sites.

In Fig. 7 we examine the possible correlation between the defect formation energy in the GB core and the GB energy. Even though the points are scattered over a wide range, the minimum defect formation energy in each GB tends to decrease with the GB energy. An extrapolation of the minimum defect formation energy to zero gives the GB energy of about 1.1–1.2 J/m^2 for both vacancies and interstitials. This number gives an estimate of the maximum possible energy of symmetrical tilt GBs in Cu. Indeed, if the defect formation energy is negative at least at one site in the GB core, the GB is unstable against a spontaneous generation of point defects at that site and should transform to a new structure.

There is another important observation that can be made from Fig. 7: while in the bulk the interstitial formation energy is much higher than the vacancy formation energy (see Table 2), in high-energy GBs both defects have comparable formation energies. This

Table 3. Energy (E_f) and entropy (S_f) of point defect formation at selected grain boundary sites. See Figs. 3–5 for site numbering.

GB	Defect	Site	E_f (eV)	S_f/k_B	Structure
$\Sigma = 5(210)[001]$	Vacancy	1-1′	0.304	2.236	Delocalized
		2-$\tilde{1}$	0.508	3.068	Delocalized
		3	1.351	1.676	Localized
	Interstitial	I	0.234	1.058	Localized
$\Sigma = 5(310)[001]$	Vacancy	1	0.623	1.355	Localized
		2	1.072	2.160	Localized
		3	1.360	0.661	Localized
		4	0.760	1.646	Localized
		5	1.009	1.528	Localized
	Interstitial	I	0.190	1.640	Localized
		I-$\tilde{1}$	0.837	2.844	Delocalized
$\Sigma = 9(1\bar{2}2)[011]$	Vacancy	1-2	0.583	2.396	Delocalized
		3	1.179	1.643	Localized
		4	1.089	1.975	Localized
		5	1.254	1.908	Localized
		7	1.308	1.394	Localized
		8	1.271	1.594	Localized
	Interstitial	I	0.756	2.901	Localized
		I	0.907	4.252	Dumbbell
$\Sigma = 11(3\bar{1}1)[011]$	Vacancy	1	1.100	1.399	Localized
		2	1.347	1.524	Localized
		3	1.280	1.570	Localized
		4	1.262	1.547	Localized
	Interstitial	I	1.490	8.019	Delocalized
		J	1.722	4.056	Localized
$\Sigma = 7(2\bar{3}1)[111]$	Vacancy	1	0.318	0.876	Localized
		2	0.867	3.403	Localized
		3	0.746	1.440	Localized
		10	1.127	2.325	Localized
		12	1.240	2.461	Localized
	Interstitial	I	0.462	1.443	Dumbbell
		J	0.885	1.971	Localized
$\Sigma = 13(3\bar{4}1)[111]$	Vacancy	1	0.185	1.185	Localized
		4	1.239	0.975	Localized
		5	0.857	2.153	Localized
		9	1.181	2.360	Localized
		11	1.145	1.783	Localized
	Interstitial	I	0.197	0.382	Dumbbell
		J	0.907	2.181	Localized

allows us to conclude that, in contrast to the bulk situation, vacancies and interstitials are equally important in GBs and should be both included in diffusion simulations.

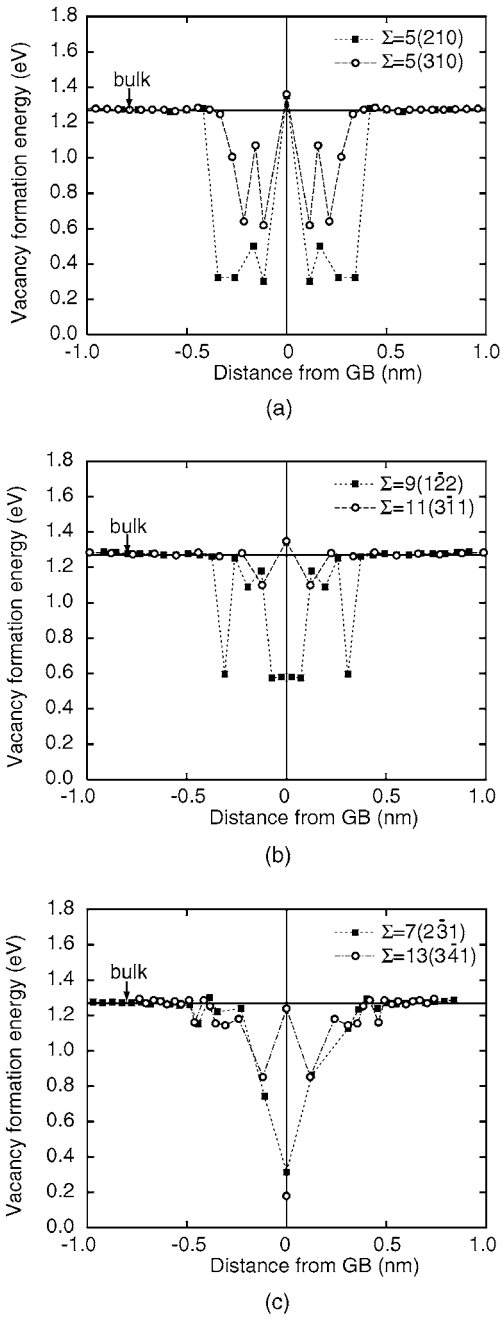

Figure 6. Vacancy formation energy as a function of the distance from the grain boundary core in Cu. (a) [001] symmetrical tilt GBs; (b) [011] symmetrical tilt GBs; (c) [111] symmetrical tilt GBs. The horizontal line indicates the vacancy formation energy in the bulk.

3.2. Grain Boundary Structure with Point Defects

The structures of GBs containing point defects have been carefully examined for the possible delocalization

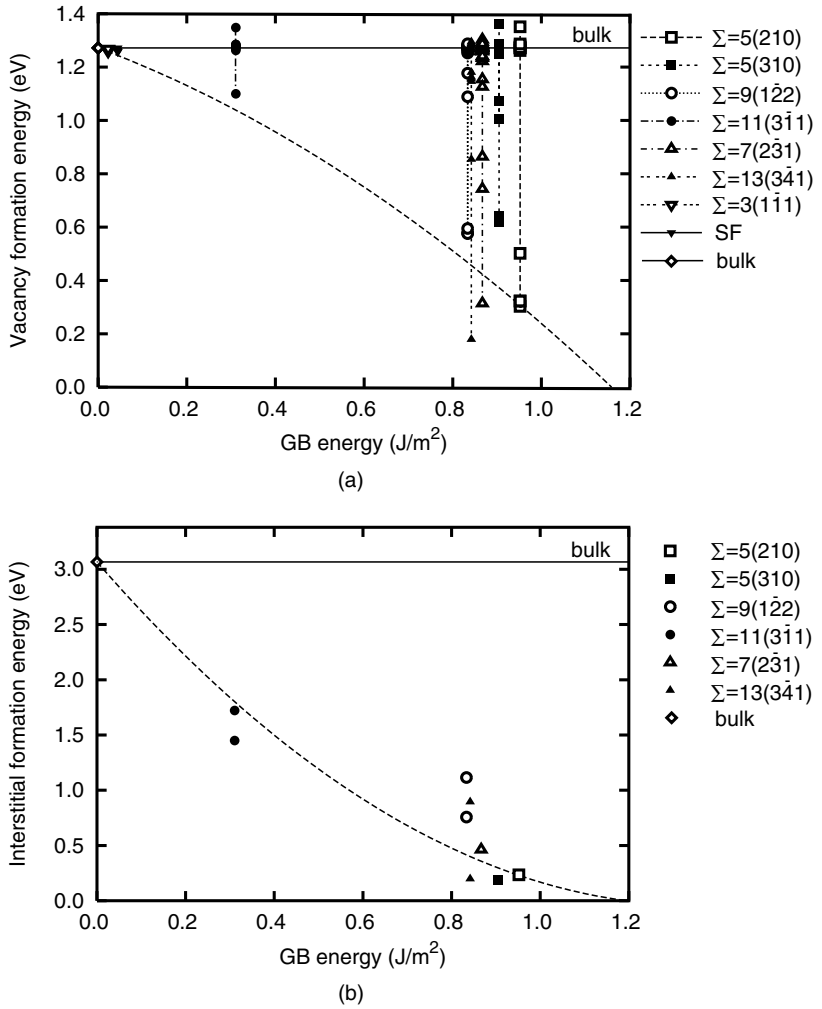

Figure 7. Point defect formation energy as a functions of grain boundary energy in Cu. (a) vacancy; (b) interstitial. The vacancy formation energies in the $\Sigma = 3(1\bar{1}1)[011]$ symmetrical twin and the intrinsic stacking fault (SF) are included for comparison. The horizontal line indicates the defect formation energy in bulk. Dashed lines show rough extrapolations through the lowest defect formation energies.

and instability effects discovered in $\Sigma = 5$ GBs [8]. The following observations have been made.

3.2.1. Vacancies in Grain Boundaries. A vacancy typically induces relatively small relaxations of neighboring atoms and remains well localized at a site where it is created. In some cases, however, the relaxations are so strong that the vacancy effectively delocalizes in the GB structure. Examples of vacancy delocalization are given in Fig. 8. When a vacancy is created at site 2 in the $\Sigma = 5(210)[001]$ GB (Fig. 8(a)), atom 1 and especially atom $\tilde{1}$ relax towards the vacant site so strongly that the free volume associated with the vacancy spreads over a relatively large region. (The tilde symbol marks an equivalent position in a neighboring structural unit.) This delocalization was also observed by Sørensen et al. [8] with a different embedded-atom potential. Similarly, when a vacancy is created at site 2 in the $\Sigma = 9(1\bar{2}2)[011]$ GB (Fig. 8(b)), the atom residing initially at site $1'$ relaxes to the midpoint between sites $1'$ and 2, which results in a vacancy delocalization between the two sites. Exactly the same configuration is obtained when we try to create a vacancy at site $1'$. Thus, by looking at the final configuration shown in Fig. 8(b) one can never tell at which site ($1'$ or 2) the vacancy was created. We believe that the vacancy delocalization is a general phenomenon which may occur in many GBs and in core regions of other extended defects.

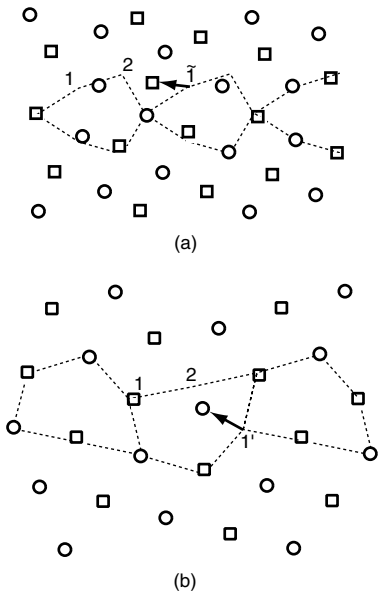

Figure 8. Examples of vacancy delocalization in Cu grain boundaries. (a) Vacancy at site 2 in the $\Sigma = 5(210)[001]$ GB. Atom 1 of the same structural unit and atom $\tilde{1}$ of the neighboring structural unit strongly relax towards the vacancy. (b) Vacancy at site 2 in the $\Sigma = 9(1\bar{2}2)[011]$ GB. Atom $1'$ strongly relaxes towards the vacancy.

Another interesting observation is the vacancy instability at certain GB sites. This effect is illustrated by four examples in Fig. 9. The first example (Fig. 9(a)) verifies the observation of Sørensen et al. [8] for the $\Sigma = 5(310)[001]$ GB: a vacancy created at site 6 is filled by atom 1 during the relaxation process. In other words, a vacancy at site 6 is absolutely unstable and spontaneously transforms to a vacancy at sites 1. Similarly, a vacancy created at site 6 in the $\Sigma = 9(1\bar{2}2)[011]$ GB (Fig. 9(b)) relaxes to a vacancy delocalized between sites $1'$ and 2. As in the previous case, site 6 does not support a stable vacancy and is filled by atom 2 in an athermal manner. In the $\Sigma = 7(2\bar{3}1)[111]$ GB (Fig. 9(c)), the unstable vacancy at sites 9 is filled by a collective jump of two atoms (1 and 2), resulting in a stable vacancy at site 1. Similarly, the unstable vacancy at site 10 in the $\Sigma = 13(3\bar{4}1)[111]$ GB (Fig. 9(d)) is filled by a collective jump of atoms $\tilde{1}$ and $\tilde{8}$, which results in a stable vacancy at site $\tilde{1}$. Table 4 gives a complete list of all GB sites that do not support a stable vacancy. We can see that the $\Sigma = 7(2\bar{3}1)[111]$ and $\Sigma = 13(3\bar{4}1)[111]$ GBs are especially prone to vacancy instability and contain only a few stable vacancy

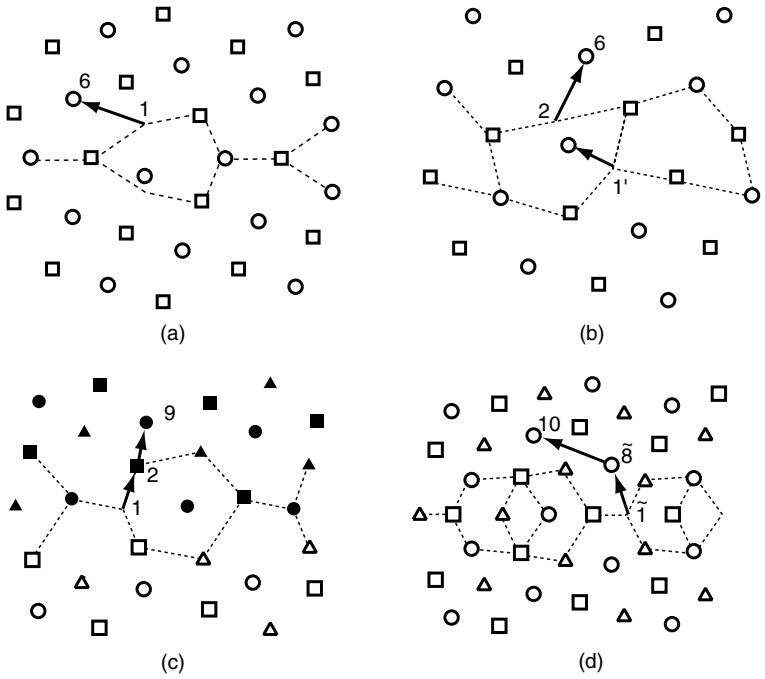

Figure 9. Examples of vacancy instability in Cu grain boundaries. (a) Unstable vacancy at site 6 in the $\Sigma = 5(310)[001]$ GB. The atom initially at site 1 fills the vacancy. (b) Unstable vacancy at site 6 in the $\Sigma = 9(1\bar{2}2)[011]$ GB. The atom initially at site 2 fills the vacancy. (c) Unstable vacancy at site 9 in the $\Sigma = 7(2\bar{3}1)[111]$ GB. The atom initially at site 2 fills the vacancy while the atom initially at site 1 simultaneously fills site 2. (d) Unstable vacancy at site 10 in the $\Sigma = 13(3\bar{4}1)[111]$ GB. The atom initially at site $\tilde{8}$ of the neighboring structural unit fills the vacancy while the atom initially at site $\tilde{1}$ simultaneously fills site $\tilde{8}$.

Table 4. Unstable vacancy sites and atomic motion during relaxation. See Figs. 3, 4 and 5 for site numbering.

GB	Site	Atomic motion
$\Sigma = 5(310)[001]$	6	1→6
$\Sigma = 9(1\bar{2}2)[011]$	6	2→6
$\Sigma = 7(2\bar{3}1)[111]$	4	1→4
	5	1→5
	6	1→6
	7	$\tilde{1}$→7
	8	1→8
	9	1→2→9
	11	1→11
	13	3→13
$\Sigma = 13(3\bar{4}1)[111]$	2	1→2
	3	$\tilde{1}$→3
	6	1→6
	7	$\tilde{5}$→7
	8	1→8
	10	$\tilde{1}$→ $\tilde{8}$→10

sites. The vacancy instability appears to be a generic phenomenon in GBs, which is probably more common than vacancy delocalization. We note that unstable vacancies were also found in near-surface layers of metals, in particular under the (110) and (111) surfaces of Cu [25, 26].

3.2.2. Interstitials in Grain Boundaries. Interstitials in GBs were found in three structural forms: (i) localized in a relatively open region ("pore"), (ii) delocalized over a relatively large area, and (iii) interstitial dumbbells. For example, the most favorable interstitial site in the $\Sigma = 5(210)[001]$ GB is the center of the triangle formed by atoms 2, 2′, and 3 (Fig. 3(a)). Interstitial atoms are strongly attracted to this site and induce only modest relaxations on neighboring atoms. Well localized interstitials with the same triangular environment were also found in the $\Sigma = 5(310)[001]$ and $\Sigma = 9(1\bar{2}2)[011]$ GBs (site I in Figs. 3(b) and 4(a)). The $\Sigma = 7(2\bar{3}1)[111]$ and $\Sigma = 13(3\bar{4}1)[111]$ GBs support a localized interstitial J above regular sites 7 and 4, respectively (Fig. 5).

Figure 10 illustrates a delocalized interstitial in the $\Sigma = 5(310)[001]$ GB. Atomic relaxations induced by the interstitial spread over two structural units and result in a configuration with two interstitials I and $\tilde{\text{I}}$ and

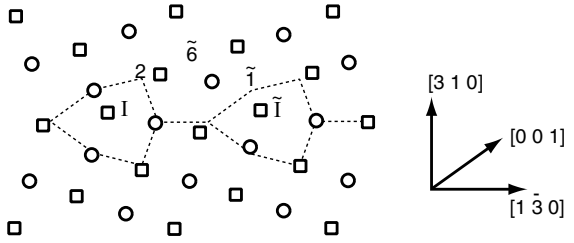

Figure 10. Delocalized interstitial in the $\Sigma = 5(310)[001]$ GB in Cu.

a vacancy delocalized between sites $\tilde{1}$, 2 and $\tilde{6}$. This configuration can be viewed as an interstitial at site I and a Frenkel pair formed by interstitial $\tilde{\text{I}}$ and a vacancy delocalized between sites $\tilde{1}$ and $\tilde{6}$. Alternatively, it can be viewed as an interstitial at site $\tilde{\text{I}}$ and a Frenkel pair formed by interstitial I and a vacancy delocalized between sites 2 and $\tilde{6}$.

Another example of a delocalized interstitial is shown in Fig. 11. When introduced at a midpoint I between sites 1 and 1* in the $\Sigma = 11(3\bar{1}1)[011]$ GB (the asterisk marks an equivalent site in a neighboring structural unit along to the tilt axis), the interstitial atom gives rise to a wide zone of significant atomic displacements parallel to the tilt axis [011]. This zone extends over 6 to 7 atomic layers on either side of the interstitial and is somewhat reminiscent of a crowdion. Although the formation energy of this highly delocalized form of an interstitial is relatively large (1.49 eV), it is highly mobile due to an extremely small migration barrier (∼0.01 eV).

Interstitials can also form split dumbbell configurations aligned either parallel or normal to the tilt axis. Dumbbells aligned normal to the tilt axis in the $\Sigma = 7(2\bar{3}1)[111]$ and $\Sigma = 13(3\bar{4}1)[111]$ GBs are illustrated in Fig. 12. In the $\Sigma = 9(1\bar{2}2)[011]$ GB, an interstitial atom localized initially at site I (Fig. 4(a)) can couple with atom 2 and, at a small energy cost, form a split dumbbell configuration oriented parallel to the tilt axis.

4. Diffusion Mechanisms in Grain Boundaries

In the previous work [8], diffusion mechanisms in $\Sigma = 5$ Cu GBs were studied by a basin constrained implementation of MD. The MD algorithm included an automated detection of defect jumps and on-the-fly evaluation of the respective jump barriers. After every jump the system was returned to the original energy basin and the simulation continued. In the present work

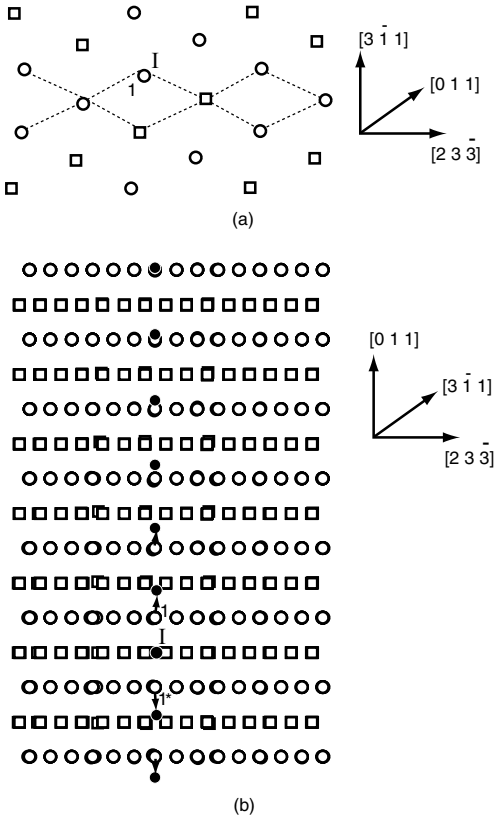

Figure 11. Delocalized interstitial atom in the $\Sigma = 11(3\bar{1}1)[011]$ GB in Cu. (a) Projection perpendicular to the tilt axis; (b) Projection parallel to the tilt axis. Symbol I indicates the position of the interstitial atom. Notice the wide zone of strong atomic displacements parallel to the tilt axis [011].

a more traditional implementation of MD was applied, which ran faster and allowed us to afford a larger simulation block (∼1200 dynamic atoms). A point defect was created at an arbitrary position in the GB core and a long MD run was implemented at a constant temperature of 1000 K. The program automatically generated snapshots at points of time when significant atomic displacement relative to a previously stored configuration pointed to a possible jump. The diffusion mechanisms were determined *a posteriori* by analyzing the whole set of snapshots which were relaxed in a static mode after the MD run. Besides defect jumps observed by MD simulations, a number of additional jumps were considered based on geometric considerations and previous experience, and their plausibility was also evaluated in the static mode as discussed below (Section 5). Typical diffusion mechanisms established this way can be summarized as follows:

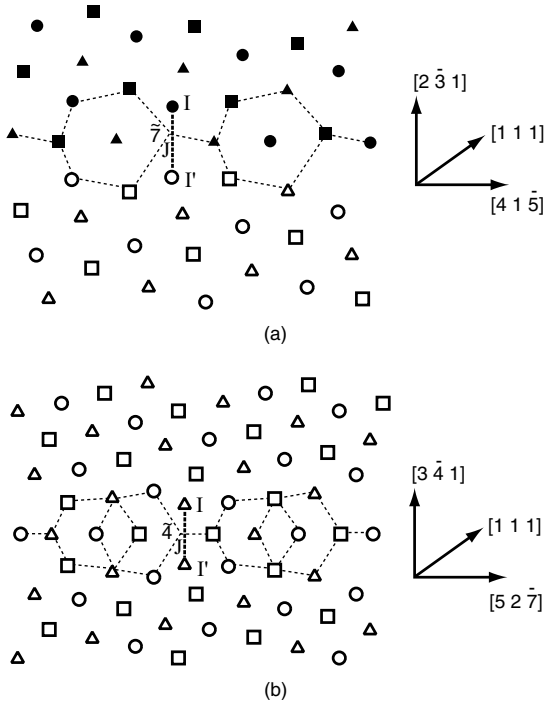

Figure 12. Interstitial dumbbells in Cu grain boundaries. (a) $\Sigma = 7(2\bar{3}1)[111]$ GB. An interstitial atom introduced near site I forms a dumbbell with an atom initially at site $\tilde{7}$. (b) $\Sigma = 7(3\bar{4}1)[111]$ GB. An interstitial atom introduced near site I forms a dumbbell with an atom initially at site $\tilde{4}$. Both dumbbells are normal to the tilt axis and to the grain boundary plane.

4.1. Vacancy Migration

In agreement with the existing paradigm, vacancies were typically found to move in GBs by exchanges with individual atoms (Fig. 13), just as they do in the bulk. However, in contrast to bulk diffusion, vacancies in GBs can also induce collective jumps of two or more atoms. Such "long" vacancy jumps always involve sites that cannot support a stable vacancy. For example, the unstable vacancy at site 6 in the $\Sigma = 5(310)[001]$ GB is responsible for the long vacancy jump $1' \to 6' \to \tilde{4}$ involving two atoms as well as for the $1 \to 6 \to \tilde{2} \to \tilde{1}$ jump involving three atoms (Fig. 13(a)). Long vacancy jumps are especially important in the $\Sigma = 7(2\bar{3}1)[111]$ and $\Sigma = 13(3\bar{4}1)[111]$ GBs in which only few sites support a vacancy. For example, the vacancy jump $5 \to 10 \to \tilde{8} \to \tilde{1}$ in the $\Sigma = 13$ GB (Fig. 13(d)) can be viewed as an attempt of a vacancy at site 5 to jump to a neighboring site 10. Since site 10 does not support a stable vacancy and should be immediately filled by a collective jump of atoms $\tilde{8}$ and $\tilde{1}$ (cf. Fig. 9(d)), the

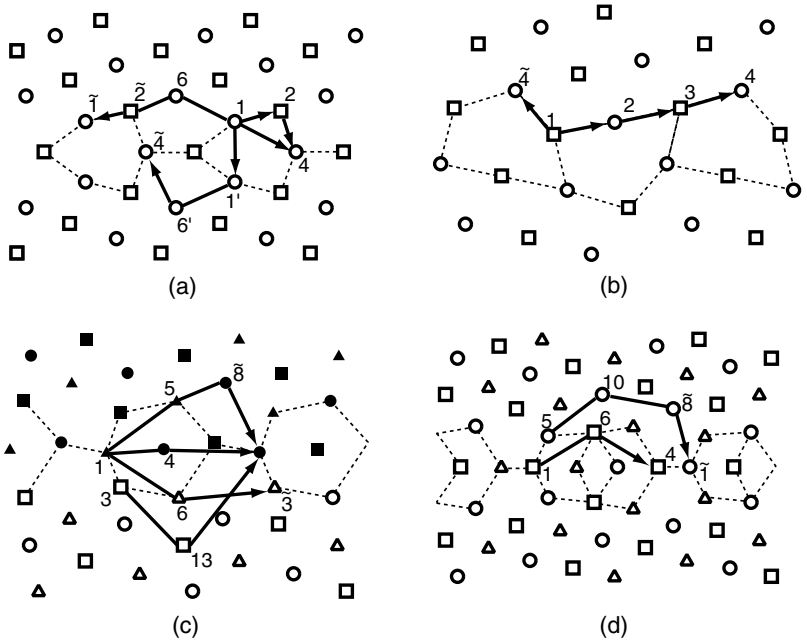

Figure 13. Vacancy jumps in selected grain boundaries in Cu. Only typical jumps included in KMC simulations are shown. (a) $\Sigma = 5(310)[001]$ GB; (b) $\Sigma = 9(1\bar{2}2)[011]$ GB; (c) $\Sigma = 7(2\bar{3}1)[111]$ GB; (d) $\Sigma = 13(3\bar{4}1)[111]$ GB. Jumps are only shown in one direction, but reverse jumps are also included in KMC simulations.

vacancy ends up at site $\tilde{1}$. The whole transition occurs by a concerted displacement of all three atoms.

Vacancy jumps parallel to the tilt axis are not shown in Fig. 13 but were also found in some of the GBs. For example, in the $\Sigma = 9(1\bar{2}2)[011]$ and $\Sigma = 11(3\bar{1}1)[011]$ GBs a vacancy at site 1 can jump to a equivalent site 1^* in a neighboring structural unit parallel to the tilt axis.

4.2. *Interstitial Migration*

Localized interstitials can move by two mechanisms: the direct mechanism and the indirect one. Under the direct mechanism an interstitial atom travels along a GB by jumping between neighboring interstitial positions. While energetically unfavorable in $\Sigma = 5$ GBs [8], this mechanism was found to operate in some other GBs studied in this work. For example, interstitial I in the $\Sigma = 9(1\bar{2}2)[011]$ GB (Fig. 4(a)) can migrate along the tilt axis by hopping directly to an equivalent site I^* in a neighboring structural unit.

Under the indirect mechanism, an interstitial atom displaces a neighboring regular atom to another interstitial position and takes its place. This process occurs by a simultaneous jump of both atoms. Furthermore, an interstitial atom can initiate a chain of atomic displacements and push out the last atom of the chain into another interstitial position, which can be well separated from the initial one. All atoms involved in this process move in a concerted manner and not one after another. Figure 14(a) and (b) illustrate this mechanism for diffusion perpendicular to the tilt axis. Notice that the same interstitial jump (e.g., $I \to \tilde{I}$ in the $\Sigma = 5(310)[001]$ GB) can be implemented in several different ways, some of them involve more atoms than others.

The four-atom jump $I \to 2 \to 6 \to \tilde{2} \to \tilde{I}$ in Fig. 14(a) actually happens in two steps, with the formation of an intermediate delocalized interstitial configuration shown in Fig. 10. Similarly, an intermediate delocalized configuration was found for the $I \to 2 \to 3 \to \tilde{I}$ jump in the $\Sigma = 9(1\bar{2}2)[011]$ GB. The indirect interstitial mechanism can also operate for diffusion parallel to the tilt axis in the [001] and [011] GBs. Especially important are the $I \to 1 \to I^*$ jump in $\Sigma = 5$ GBs and the $I \to 2 \to I^*$ jump in the $\Sigma = 9(1\bar{2}2)[011]$ GB, although other indirect jumps parallel to the tilt axis can play a role too. No indirect interstitial jumps parallel to the tilt axis were found in [111] GBs.

An interstitial dumbbell always moves by a collective jump of three or more atoms, as it does also in

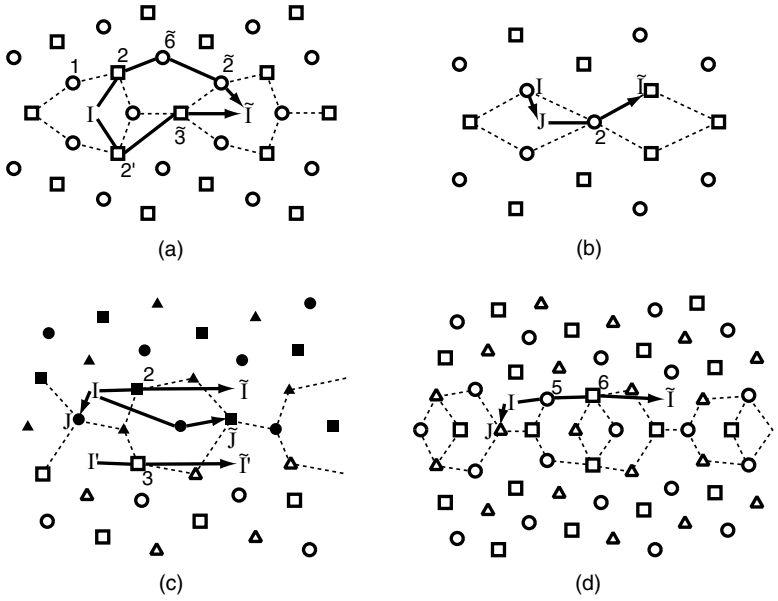

Figure 14. Interstitial jumps in selected grain boundaries in Cu. Only typical jumps included in KMC simulations are shown. (a) $\Sigma = 5(310)$ GB; (b) $\Sigma = 11(3\bar{1}1)$ GB; (c) $\Sigma = 7(2\bar{3}1)$ GB; (d) $\Sigma = 13(3\bar{4}1)$ GB.

the bulk. For example, the dumbbell jumps shown in Fig. 14(c) and (d) involve five or six atoms. A dumbbell can also transform into a localized configuration J, followed by its split into a dumbbell one (111) layer deeper. Repeated transformations of this type can make an important contribution to diffusion parallel to the tilt axis.

Finally, the highly delocalized interstitial I in the $\Sigma = 11(3\bar{1}1)[011]$ GB (Fig. 11) can migrate along the tilt axis with an extremely small activation barrier. Each step of this motion is accompanied by a very small displacement of each individual atom, yet the entire relaxation zone translates by one period. Alternatively, the interstitial atom located in the center of the displacement zone can jump to a type-J position (Fig. 4(b)) and become a localized interstitial.

5. Calculation of Defect Concentrations and Rate Constants

Diffusion calculations require a knowledge of point defect concentrations in GBs. Assuming that such concentrations are small, the fraction of time that a particular site α in the GB core is occupied by a defect (vacancy or interstitial) can be calculated by

$$c_\alpha = \exp\left(-\frac{E_f^\alpha - TS_f^\alpha}{k_B T}\right), \tag{4}$$

where E_f^α and S_f^α are the defect formation energy and entropy at site α.

Rate constants calculations of defect jumps present a more difficult task. The absolute rate $\Gamma_{\alpha\beta}$ of a particular defect jump $\alpha \to \beta$ (jump probability per unit time) can be calculated from the transition state theory expression [27]

$$\Gamma_{\alpha\beta} = \nu_0^{\alpha\beta} \exp\left(\frac{-E_m^{\alpha\beta}}{k_B T}\right). \tag{5}$$

Here $E_m^{\alpha\beta}$ is the migration energy (energy barrier) defined as the difference in energy between the transition state and the initial state, and $\nu_0^{\alpha\beta}$ is the attempt frequency of the jump given by

$$\nu_0^{\alpha\beta} = \frac{\prod_{i=1}^{3N} \nu_i}{\prod_{i=1}^{3N-1} \nu_i^*}, \tag{6}$$

where ν_i are normal vibrational frequencies in the initial state and ν_i^* are such frequencies at the saddle point. The dominator of this expression contains one frequency less than the numerator because, as we approach the transition state, one vibrational degree of freedom converts to a translational one representing the motion of our system along the reaction path.

The main challenge of rate constant calculations is finding the saddle point configuration of a defect jump.

Earlier calculations were based on the "drag" method [6, 7, 9, 10] in which an atom making a jump was moved from the initial to the final position by small steps with a constrained relaxation after each step. The "drag" method proved to be very efficient in many diffusion calculations but it has the drawback that only single-atom jumps can be simulated. This method would be inadequate for the purposes of our work since many defect jumps in GBs involve collective motion of atomic groups. More advanced methods of saddle point search have recently been reviewed by Henkelman et al. [28]. In the present work we used the nudged elastic band (NEB) method [28, 29] which had been successful in simulating a variety of rate processes, including GB diffusion [8].

Even though the transition-state theory expressions (5) and (6) involve only the initial and transition states but not the final state of the jump, in the NEB method both the initial and final states should be known. The method proceeds as follows. All atoms in the simulation block should be labeled. The first step is to create a set of copies (or "images") of the system which initially represent intermediate states of the jump. This can be achieved by a linear interpolation of atomic coordinates between the initial and final states. The total energy of this set of images, called the "elastic band", is defined as the sum of potential energies of individual images due to interatomic forces plus a fictitious energy of elastic deformation of imaginary springs connecting the images. This total energy is minimized with respect to atomic displacements in all images. At each iteration of the minimization process, some components of the interatomic and elastic forces are turned to zero ("nudging") in order to accelerate the convergence. It can be shown that the relaxed elastic band should position itself approximately along the minimum energy path going through the saddle point. Therefore, the saddle-point configuration can be approximated by the image with the highest potential energy along the elastic band. Furthermore, an interpolation of atomic coordinates between the maximum-energy image and its neighbors can be applied to locate the saddle point more accurately. This procedure is clearly not restricted to single-atom jumps and equally applies to any collective transformation.

There is one aspect of the calculation that should be discussed here in more detail since it affects the rate constants delivered by the method. The relaxation of the elastic band was performed in this work under a constant volume corresponding to the initial state of the jump (GB with a single point defect). Since the saddle-point configuration often has a more open structure than the initial state, by moving our system to the saddle point we increase the hydrostatic pressure in the block by a small amount Δp. The effect of a small change in pressure on the jump barrier $E_m^{\alpha\beta}$ is negligible, but the effect on the attempt frequency can be more significant [30]. Indeed, a change in pressure affects vibrational frequencies of atoms and thus alters the vibrational entropy of the system at the saddle point by a small amount ΔS. This, in turn, leads to a change in the attempt frequency $\nu_0^{\alpha\beta}$ by a factor of $\exp(\Delta S/k_B)$. In order to recover the true value of the attempt frequency, $\nu_0^{\alpha\beta}$ determined under a constant volume should be multiplied by a factor of $\exp(-\Delta S/k_B)$. Applying the thermodynamic relation $(\partial S/\partial p)_T = -\beta V$ (S being the system entropy) [31], the following linear relation should hold between ΔS and Δp [30]:

$$\Delta S = -\beta V \Delta p, \tag{7}$$

where V is the system volume and β is the volume coefficient of thermal expansion defined by $\beta = V^{-1}(\partial V/\partial T)_p$. The latter was determined for Cu by computing the vibrational entropy ΔS of a perfect lattice block as a function of pressure p and extrapolating the ratio $\Delta S/pV$ to $p = 0$. This calculation gives $\beta = 4.458 \times 10^{-5}\ \mathrm{K}^{-1}$. It should be remembered that the product pV (and thus the pressure p) can be readily calculated within the embedded atom method for any atomic configuration [30]. For a defect jump in a GB, the excess pressure at the saddle point equals $\Delta p = p^* - p_0$, where p^* is the pressure at the saddle point and p_0 is the pressure before the jump.[2] Thus, Eq. (6) for the attempt frequency should be modified as follows:

$$\nu_0^{\alpha\beta} = \frac{\prod_{i=1}^{3N} \nu_i}{\prod_{i=1}^{3N-1} \nu_i^*} \exp\left[\frac{\beta(p^* - p_0)V}{k_B}\right], \tag{8}$$

with vibrational frequencies determined under constant volume conditions. Equation (8) was applied for attempt frequency calculations in GBs throughout this work. The same equation with $p_0 = 0$ was also used in bulk calculations reported in Table 2.

6. Calculation of Diffusion Coefficients

For each GB and each type of point defect, a catalog of the most favored jumps has been created based on two

criteria. First, jumps with relatively low partial activation energy $E_{\alpha\beta} = E_f^{\alpha} + E_m^{\alpha\beta}$ have been selected. Indeed, the average number of $\alpha \to \beta$ jumps per unit time is proportional to $c_\alpha \Gamma_{\alpha\beta} \propto \exp[-(E_f^{\alpha} + E_m^{\alpha\beta})/k_B T]$, suggesting that jumps with lower values of $E_{\alpha\beta}$ should occur more often and that the partial activation energy can be used for ranking the relative importance of jumps [8]. Second, the jumps included in the catalog should form a penetrating network capable of supporting a macroscopic diffusion flux in any direction in the GB plane. The number of favored jumps selected for each GB depends sensitively on the GB structure and varies between 2 and 9 for the vacancy mechanism and between 3 and 7 for the interstitial mechanism (not counting the jump reversals which, of course, were also included in the catalog). Some of the favored jumps are shown in Figs. 13 and 14.

The set of defect concentrations c_α and the catalog of rate constants $\Gamma_{\alpha\beta}$ at a given temperature T form the input data set for calculating the GB diffusion coefficient by KMC simulations. The KMC procedure applied in this work was similar to the one developed by Sørensen et al. [8]. In short, a large simulation block is created with periodic boundaries in two directions parallel to the GB plane and the thickness of the GB core in the third direction. The GB structure is mapped onto this block, all atoms of the block are labeled, and a single point defect is created at an arbitrary site. The defect starts to wander along the GB by implementing random jumps drawn from the catalog. At each step, we calculate the residence time of the defect at its current site α,

$$\tau_\alpha = \frac{1}{\sum_{\beta=1}^{k_\alpha} \Gamma_{\alpha\beta}},$$

as well as the jump probabilities

$$P_{\alpha\beta} = \tau_\alpha \Gamma_{\alpha\beta}$$

for all k_α jumps that can be made form that site. The jump direction is decided by generating a random number. The chosen jump is implemented by moving atoms involved in the jump, the clock is advanced by τ_α, and the simulation continues. As the defect walks through the GB, it moves atoms around and thereby induces their diffusion. The defect walk consists of a fixed number of jumps and is repeated a large number m of times. Once the simulation is complete, the diffusion coefficient D in a given direction in the GB plane is determined from the random walk theory equation [8]

$$D = \frac{C_d \sum_{k=1}^{m} \sum_{\gamma=1}^{N} \chi_{\gamma k}^2}{2Mt}, \tag{9}$$

where M is the number of atoms in the simulation block, $\chi_{\gamma k}$ is the projection of the total displacement vector of the γ-th atom resulting from k-th walk, and t is the total simulation time. In Eq. (9),

$$C_d = \sum_{\alpha} c_\alpha$$

(where the summation runs over all defect sites available in the simulation block) is the average number of defects that would be found in the block under equilibrium conditions. Factor C_d in Eq. (9) makes a correction for the fact that the simulation block contains exactly one defect at all temperatures, which does not necessarily coincides with the equilibrium defect concentration.

The accuracy of the diffusion coefficient determined from Eq. (9) is extremely high because every jump attempt is successful and therefore large statistics of jumping can be readily accumulated. In this work, the KMC block typically contained $M = (2 \text{ to } 4) \times 10^4$ atoms. The total number of defect jumps used for calculating the diffusion coefficient varied between 10^{10} and 10^{11}.

The KMC simulations were carried out in the temperature range 500–1100 K. The diffusion coefficients in each GB, plotted in the Arrhenius format log D versus $1/T$, give fairly linear as illustrated in Fig. 15. The

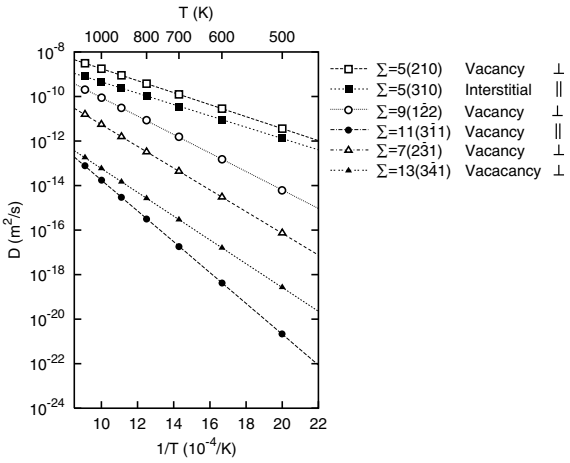

Figure 15. Arrhenius plots of grain boundary diffusion coefficients in Cu obtained by KMC simulations. Only the fastest diffusion coefficient is shown for each direction in each grain boundary.

Table 5. Arrhenius parameters of grain boundary diffusion in Cu obtained by fitting Eq. (10) to KMC results.

		Parallel to the tilt axis		Normal to the tilt axis	
GB	Mechanism	Q (eV)	D_0 (m^2/s)	Q (eV)	D_0 (m^2/s)
$\Sigma = 5(210)[001]$	Vacancy	0.532	3.72×10^{-7}	0.529	6.74×10^{-7}
	Interstitial	0.757	8.95×10^{-7}	0.859	3.65×10^{-6}
$\Sigma = 5(310)[001]$	Vacancy	1.172	1.45×10^{-6}	1.210	3.27×10^{-6}
	Interstitial	0.505	1.59×10^{-7}	0.759	6.41×10^{-7}
$\Sigma = 9(1\bar{2}2)[011]$	Vacancy	0.906	3.57×10^{-6}	0.823	1.26×10^{-6}
	Interstitial	1.085	7.36×10^{-6}	1.091	3.49×10^{-6}
$\Sigma = 11(3\bar{1}1)[011]$	Vacancy	1.373	1.46×10^{-7}	1.710	1.10×10^{-6}
	Interstitial	1.569	1.59×10^{-6}	2.126	2.67×10^{-5}
$\Sigma = 7(2\bar{3}1)[111]$	Vacancy	0.972	2.45×10^{-7}	0.969	4.17×10^{-7}
	Interstitial	1.201	2.58×10^{-6}	1.171	3.18×10^{-6}
$\Sigma = 13(3\bar{4}1)[111]$	Vacancy	1.120	4.24×10^{-9}	1.060	1.28×10^{-8}
	Interstitial	1.201	7.37×10^{-7}	1.340	2.50×10^{-7}

plots do have some curvature, but it is relatively small and cannot be noticed in comparison with the wide (4–8 orders of magnitude) range of D values covered by the calculations. Considering the linearity of the plots, the diffusion coefficients were fit by the Arrhenius equation

$$D = D_0 \exp\left(-\frac{Q}{k_B T}\right), \tag{10}$$

which gave us the activation energy Q and pre-exponential factor D_0 for diffusion in each GB. The Arrhenius parameters are summarized in Table 5.

7. Discussion and Conclusions

By comparing the relevant diffusion coefficients, the mechanisms that dominate diffusion parallel and perpendicular to the tilt axis have been identified for each GB. The dominant diffusion mechanisms are listed in Table 6 and the relevant Arrhenius plots are shown in Fig. 15. We notice that diffusion in the $\Sigma = 5(310)[001]$ GB is dominated by the interstitial mechanism whereas diffusion in all other GBs is dominated by vacancies. This result suggests that there is no universal mechanism of GB diffusion and that the latter can be dominated by either vacancies or interstitials, depending on the GB structure. It is interesting to notice that most of the previous work in this area has been done on the $\Sigma = 5(310)[001]$ GB which has been considered as a "typical" high-angle GB. Table 6 demonstrates that, ironically, this GB is more an exception than a rule, at least as far as point defects and diffusion are concerned. This GB has an extremely high affinity for the interstitial formation in the center of the capped trigonal prism (Fig. 3(b)) with very low formation and migration energies of the interstitial (cf. Table 3).

Table 6. Dominant diffusion mechanism in Cu grain boundaries for diffusion parallel and normal to the tilt axis. The bold typeset indicates the fastest diffusion direction.

GB	Parallel	Normal
$\Sigma = 5(210)[001]$	Vacancy	**Vacancy**
$\Sigma = 5(310)[001]$	**Interstitial**	Interstitial
$\Sigma = 9(1\bar{2}2)[011]$	Vacancy	**Vacancy**
$\Sigma = 11(3\bar{1}1)[011]$	**Vacancy**	Vacancy
$\Sigma = 7(2\bar{3}1)[111]$	Vacancy	**Vacancy**
$\Sigma = 13(3\bar{4}1)[111]$	Vacancy	**Vacancy**

Another interesting observation is that diffusion parallel to the tilt axis can be faster or slower than diffusion normal to the tilt axis, depending on the GB structure (Table 6). This is contrary to the common view that diffusion parallel to the tilt axis should always be faster. The latter relation should indeed be expected, and was observed experimentally [32], for low-angle GBs composed of an array of dislocations parallel to the tilt axis. As far as high-angle GBs are concerned, "special" low-Σ GBs have a less anisotropic structure and the tilt axis does not have to be the preferred diffusion direction in all cases. It is this type of GBs that were studied in this

work. On the other hand, so-called "vicinal" GBs with tilt angles slightly away from a "special" orientation contain an array of misfit dislocations running parallel to the tilt axis in the otherwise "special" structure [4]. The misfit dislocations can enhance diffusion parallel to the tilt axis and thereby alter the diffusion anisotropy in favor of that direction. Even if diffusion normal to the tilt axis is faster in the "special" structure, as it is for example in the $\Sigma = 7$ and $\Sigma = 13$ GBs, deviations of the tilt angle from the ideal orientation may reverse the sense of the anisotropy and make diffusion parallel to the tilt axis faster. This was likely to be the case in the recent experimental measurements on [001]-oriented Ag bicrystals in which diffusion parallel to the tilt axis was found to be faster than in the normal direction for all tilt angles studied, including angles close (but presumably not identical) to the ideal $\Sigma = 5(310)$ and $\Sigma = 5(210)$ GBs [33].

Figure 16 shows the spectra of partial activation energies of vacancy and interstitial jumps included in the KMC simulations. The effective activation energies deduced by fitting the respective Arrhenius plots are also shown for comparison. The comparison does not support the view, expressed often in the past, that GB diffusion is dominated by the easiest jumps, i.e., defect jumps with the lowest partial activation energy. Generally, GB diffusion depends on many different jumps in a complex way as well as on the GB structure through jump-correlation effects, which are more significant in GBs than they are in a regular lattice [2, 3, 8, 34, 35]. The easiest jumps alone may be unable to support a macroscopic diffusion flux if they do not form a two-dimensional[3] network penetrating through the GB structure, which is often the case in GBs. A careful examination of the six GBs studied in this work shows that there is always a jump, or a group of jumps with nearby partial activation energies, which provide a two-dimensional network that controls the rate of the overall diffusion process. This explains why the Arrhenius law is followed by GB diffusion so accurately. However, such "leading" jumps do not always coincide with the easiest jumps and often have partial activation energies lying deep inside the spectrum (Fig. 16). This fact points to the importance of considering a large set of defect jumps for a reliable calculation of diffusion coefficients.

Years ago, Borisov et al. [36] and Gupta [37] suggested, based on general thermodynamic considerations, a linear correlation between the activation energy of GB diffusion and the GB energy, with lower

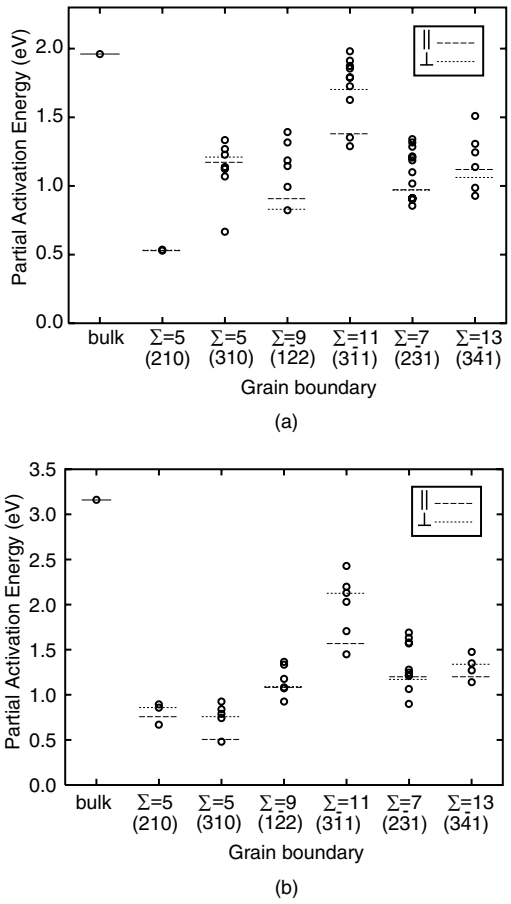

Figure 16. Partial activation energies of defect jumps included in KMC simulations. (a) vacancy mechanism; (b) interstitial mechanisms. Dashed lines indicate effective activation energies of diffusion parallel (∥) and perpendicular (⊥) to the tilt axis calculated by fitting Eq. (10) to KMC results.

activation energies in high-energy GBs. While experimental data generally follow this rule, it has never been examined by atomic-level calculations. In Fig. 17, the activation energies of diffusion in the six GBs calculated in this work are plotted against the GB energy. Despite the significant scatter of the points, the lowest activation energy in each GB seems to follow the Borisov rule. The anisotropy of the activation energy makes a linear correlation somewhat fuzzy, but the trend for high-energy GBs to have lower activation energies appears to be persistent. Further calculations are needed for a more rigorous test of the linear relation.

In conclusion, our calculations for six symmetrical tilt GBs in Cu confirm that the basic results obtained by Sørensen et al. [8] for $\Sigma = 5$ GBs are general and

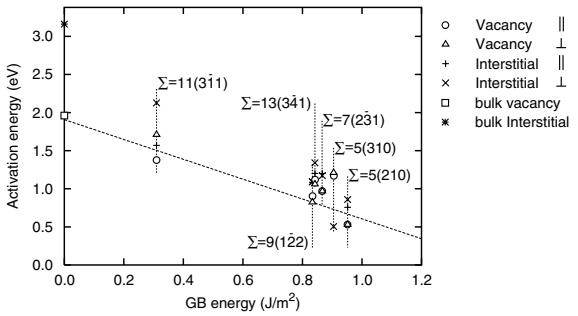

Figure 17. The activation energy of diffusion parallel (∥) and perpendicular (⊥) to the tilt axis in Cu grain boundaries. The activation energy of diffusion in the perfect lattice is shown for comparison. The dashed line is a linear extrapolation through the minimum activation energies in different grain boundaries.

hold for other GBs as well. For the $\Sigma = 5$ GBs, our calculations with a different embedded-atom potential verify the main results of Ref. [8] despite slight differences in numerical values of the diffusion constants. GBs are able to support localized vacancies and interstitials at certain sites, but there are sites that do not support a stable vacancy. Furthermore, vacancies and interstitials can delocalize in the GB structure by inducing strong atomic displacements extending over a large area. A similar effect was earlier reported by Vitek et al. [38] who observed local structural transformations induced by vacancies at selected GB sites in fcc and bcc metals. Interstitials can also form split dumbbell configurations as they do in the lattice. All these effects appear to be general and are expected to be present in many GBs as well as in core regions of other extended defects. In contrast to a regular lattice where interstitial atoms have extremely low concentrations and do not normally contribute to self-diffusion, both vacancies and interstitials are equally important in GBs and can both contribute to GB diffusion. Vacancies can move in GBs by single-atom exchanges or by "long" jumps involving a collective displacement of several atoms. Interstitials can move by direct jumps between interstitial positions or by collective processes involving 2–4 atoms. The dominant diffusion mechanism can be different in different GBs. GB diffusion coefficients follow the Arrhenius law with an effective activation energy that often correlates with the partial activation energy of a certain defect jump or a group of jumps with close activation energies, but not necessarily with the easiest jump. Diffusion in tilt GBs is anisotropic, but diffusion parallel to the tilt axis can be faster or slower than diffusion normal to the tilt axis, depending on the GB structure. The activation energy of GB diffusion in the fastest direction tends to decrease with the GB energy.

Acknowledgments

This work was supported by the US Department of Energy (Office of Basic Energy Sciences) under a Grant No. DE-FG02-01ER45871.

Notes

1. This is only true in the classical harmonic approximation. Quantum effects and lattice anharmonicity may lead to temperature-dependent S_f^α values.
2. Because the block sizes in directions parallel to the GB are fixed at their perfect-lattice values, the interfacial tension of the GB creates a residual pressure in the block that cannot be eliminated by relaxation. This explains why $p_0 \neq 0$ for a GB block with or without a point defect.
3. One-dimensional easy-jump channels, if isolated from one another, are not efficient for diffusion because the jump correlation factor for defect-mediated diffusion in one-dimensional systems is zero [34, 35]. The direct interstitial mechanism is the only exception to this rule.

References

1. I. Kaur, Y. Mishin, and W. Gust, *Fundamentals of Grain and Interphase Boundary Diffusion* (Wiley, Chichester, 1995).
2. Y. Mishin, Defect Diffus. Forum **143–147**, 1357 (1997).
3. Y. Mishin, Defect Diffus. Forum **194–199**, 1113 (2001).
4. A.P. Sutton and R.W. Balluffii, *Interfaces in Crystalline Materials* (Clarendon Press, Oxford, 1995).
5. R.W. Balluffi, in *Diffusion in Crystalline Solids*, edited by G.E. Murch and A.S. Nowick (Academic Press, New York, 1984), pp. 319–377.
6. Q. Ma, C.L. Liu, J.B. Adams, and R.W. Balluffi, Acta Metall. Mater. **41**, 143 (1993).
7. C.L. Liu and S.J. Plimpton, Phys. Rev. B **51**, 4523 (1995).
8. M.R. Sørensen, Y. Mishin, and A.F. Voter, Phys. Rev. B **62**, 3658 (2000).
9. M. Nomura and J.B. Adams, J. Mater. Res. **7**, 3202 (1992).
10. M. Nomura and J.B. Adams, J. Mater. Res. **10**, 2916 (1995).
11. Y. Mishin, M.J. Mehl, D.A. Papaconstantopoulos, A.F. Voter, and J.D. Kress, Phys. Rev. B **63** (2001).
12. Y. Mishin, D. Farkas, M.J. Mehl, and D.A. Papaconstantopoulos, Phys. Rev. B **59**, 3393 (1999).
13. V. Vitek, Crystal Lattice Defects **5**, 1 (1974).
14. Y. Mishin and D. Farkas, Philos. Mag. *A* **78**, 29 (1998).
15. J.M. Howe, *Interfaces in Materials* (John Wiley, NY, 1997).
16. D. Wolf and S. Yip (Eds.), *Materials Interfaces: Atomic-Level Structure and Properties* (Chapman and Hall, London, 1992).
17. P. Keblinski, D. Wolf, S.R. Phillpot, and H. Gleiter, Philos. Mag. A **79**, 2735 (1999).

18. J.D. Rittner and D.N. Seidman, Phys. Rev. B **54**, 6999 (1996).
19. J.R. Hu, S.C. Chang, F.R. Chen, and J.J. Kai, Scripta Mater. **45**, 463 (2001).
20. W. Hu, D.A. Molodov, B. Schönfelder, L.S. Shvindlerman, and G. Gottstein, Interface Science **8**, 335 (2000).
21. R.W. Siegel, J. Nucl. Mater. **69–70**, 117 (1978).
22. R.W. Balluffi, J. Nucl. Mater. **69–70**, 240 (1978).
23. H. Ullmaier (Ed.), *Properties and Interaction of Atomic Defects in Metals and Alloys*, *Landolt-Bornstein, New Series, Group III* (Springer, Berlin, 1991), Vol. 25, p. 88.
24. F.W. Young, J. Nucl. Mater. **69–70**, 310 (1978).
25. R.N. Barnett and U. Landman, Phys. Rev. B **44**, 3226 (1991).
26. F. Willaime, Y. Piquet, and B. Legrand, Defect and Diffusion Forum **194–199**, 1381 (2001).
27. G.H. Vineyard, J. Phys. Chem. Solids **3**, 121 (1957).
28. G. Henkelman, G. Johannesson, and H. Jonsson, in *Theoretical Methods in Condensed Phase Chemistry*, edited by S.D. Schwartz, *Progress in Theoretical Chemistry and Physics*, Ch. 10, Kluwer Academic Publishers (2000), Vol. 5.
29. H. Jónsson, G. Mills, and K.W. Jacobsen, in *Classical and Quantum Dynamics in Condensed Phase Simulations*, edited by B.J. Berne, G. Ciccotti, and D.F. Coker (World Scientific, Singapore, 1998).
30. Y. Mishin, M.R. Sørensen, and A.F. Voter, Philos. Mag. A **81**, 2591 (2001).
31. E.A. Guggenheim, *Thermodynamics. An Advanced Treatment for Chemistis and Physicists* (Elsevier Science, North Holland, 4th ed., 1993).
32. R.E. Hoffman, Acta Metall. **4**, 56 (1956).
33. J. Sommer, Chr. Herzig, S. Mayer, and W. Gust, Defect Diff. Forum **66–69**, 843 (1989).
34. Y. Mishin and Chr. Herzig, Phil. Mag. A **71**, 641 (1995).
35. Y. Mishin, Philos. Mag. A **72**, 1589 (1995).
36. V.T. Borisov, V.M. Golikov, and G.V. Scherbedinsky, Phys. Met. Metallogr. **17**, 80 (1964).
37. D. Gupta, Metall. Trans. A **8**, 1431 (1977).
38. V. Vitek, Y. Minonishi, and G.J. Wang, J. de Physique **46**, 171 (1985).